Exposure accumulation drives age-dependent disease architectures and polygenic risk scores

Xilin Jiang[1,2,3,4,5,*], Alkes L. Price[3,4,6], John Danesh[1,2,7,8,9,10], Gil McVean[11], Michael Inouye[1,2,7,9,12,13], Sarah Urbut[4,14], Arun Durvasula[15,16,17,*]

1. British Heart Foundation Cardiovascular Epidemiology Unit, Department of Public Health and Primary Care, University of Cambridge, Cambridge UK
2. Victor Phillip Dahdaleh Heart and Lung Research Institute University of Cambridge, Cambridge UK
3. Department of Epidemiology, Harvard T.H. Chan School of Public Health Boston MA USA
4. Broad Institute, Cambridge, MA USA
5. Cambridge Centre for AI in Medicine, University of Cambridge, Cambridge UK
6. Department of Biostatistics, Harvard T.H. Chan School of Public Health Boston MA USA
7. British Heart Foundation Centre of Research Excellence, University of Cambridge, Cambridge, UK
8. National Institute for Health and Care Research Blood and Transplant Research Unit in Donor Health and Behaviour, University of Cambridge, Cambridge, UK
9. Health Data Research UK Cambridge, Wellcome Genome Campus and University of Cambridge, Cambridge, UK
10. Department of Human Genetics, Wellcome Sanger Institute, Hinxton, UK
11. Ellison Institute of Technology, Oxford, UK
12. Cambridge Baker Systems Genomics Initiative, Department of Public Health and Primary Care, University of Cambridge, Cambridge, UK
13. Cambridge Baker Systems Genomics Initiative, Baker Heart and Diabetes Institute, Melbourne, Victoria, Australia
14. Cardiology Division, Massachusetts General Hospital, Boston, MA USA.
15. Division of Epidemiology, Department of Population and Public Health Sciences, Keck School of Medicine, University of Southern California, Los Angeles, CA
16. Center for Genetic Epidemiology, Department of Population and Public Health Sciences, Keck School of Medicine, University of Southern California, Los Angeles, CA
17. Department of Quantitative and Computational Biology, University of Southern California, Los Angeles, California, USA

* Correspondence: xj262@medschl.cam.ac.uk (XJ); arun.durvasula@med.usc.edu (AD)

Abstract

Our understanding of the dependence of the genetic and environmental architecture of common diseases on age is incomplete. Here, we use longitudinal data to quantify age-dependent genetic and environmental components of complex traits and diseases. When applying our approach to 16 UK Biobank quantitative traits (average N=180K), we found environmental variance can accumulate with age, which leads to decreasing heritability with age, following an exposure accumulation model. We find heritability decreases with age for 5 traits, including systolic blood pressure and lung function (FEV1/FVC), with an average change of −17.8% with age per 10-years. When analyzing complex diseases, we found evidence that environmental variance in disease liability also accumulates with age for 5 of 9 diseases, with an average decrease of heritability −18.1% per 10 years. We found a liability-threshold model with exposure accumulation explains 86% of decreasing PRS prediction R^2 with age in 9 UK Biobank complex diseases. Finally, we show that both genetic and non-genetic predictors have decreasing prediction accuracy with age in 61 predictor-disease pairs, consistent with simulations. Our results suggest ascertaining younger cohorts is more powerful for training both genetic and non-genetic risk prediction models.

Introduction

The extent to which genetics and environmental exposures interact with age when contributing to phenotypic variation in a population is unclear. Previous studies have found evidence that environmental exposures can account for more phenotypic variation in older individuals, potentially due to the accumulation of exposures as people age[1–3]. However, measuring the relevant environmental exposures throughout an individual's lifetime remains a significant challenge. On the other hand, gene-age interaction, which can arise from multiple sources[4], including proportional amplification of genetic variance[5] and different age profiles of genetic effects across genotypes[6], could drive age-dependent phenotypic variation. Jointly studying the age profiles of genetic and non-genetic components of complex traits can elucidate the architectures of age-dependent complex traits.

Recent work has shown age-varying prediction accuracy for polygenic risk scores (PRS), but whether this observation is driven by gene-age interactions or other mechanisms is unknown[6–12]. Significant challenges remain in studying age-dependent disease architectures. First, disease liability is not observed and performing gene-age interaction tests on binary disease observations may not be informative of interactions on the liability scale[13]. Second, although methods exist reduce bias in modeling time-to-event data due to censoring, these methods often have assumptions that are not met in empirical data[6].

Here, we estimated the age-dependent profiles of genetic and environment components of complex traits and disease liability. We show that the impact of environmental exposures accumulates with age for a wide range of complex traits and diseases, which causes a decrease in heritability with age. We show that exposure accumulation, under a liability-threshold model[14,15], explains decreasing prediction accuracy of PRS prediction accuracy for 9 diseases in UK Biobank. Finally, we show by simulation and analytical derivation that a liability-threshold model predicts that both genetic and environmental factors will have decreased prediction accuracy for older cases, which we validate in empirical data using 61 predictor-disease pairs.

Results

Overview of methods

We study age-dependent trait architecture under an exposure accumulation (EA) model where liability is linear in genetic, environment, and age quintiles[16], with environmental variance accumulating with age.

The EA model can be formalized under the following:

$$L = G + E + age + \sum_{a=0}^{age} E_a, \quad (1)$$

where L denotes liability, G is the genetic component of liability, E is the environmental component, age is the quintile of age, and E_a is the contribution of age to liability. $\sum_{a=0}^{age} E_a$ is the term arising from the EA model. We study architecture across age quintiles to relax statistical assumptions on the relationship between age and L. We evaluate evidence for 4 additional models that can cause an age-dependent architecture: proportional amplification[5,13] (ref), age-dependent G, exposure accumulation with decay, and non-proportional amplification (**Supplementary Table 1**).

We evaluate evidence of the EA model by estimating age-varying heritability ($\Delta h^2 = h^2_{older} - h^2_{younger}$), which is negative under the EA model. We estimate Δh^2 by estimating the heritability for each age quintile with BOLT-REML[17] and fitting a model where heritability changes linearly with age. We estimate heritability with age and sex as covariates to account for within age quintile variation due to age and sex. We test for non-zero Δh^2 with a likelihood ratio test between the model with age term and a null model where heritability is constant with age. We also evaluate the environmental correlation between age quintiles ($\rho(E_{younger}, E_{older})$), which is expected to be less than 1.0 under the EA model. We use phenotypic correlations (ρ_l), which is an upper bound of $\rho(E_{younger}, E_{older})$ under the EA model, to evaluate evidence of $\rho(E_{younger}, E_{older}) < 1$. We account for error-in-measurement of ρ_l by computing the denoised phenotypic correlation ($\tilde{\rho}_l$) for individuals with three phenotype measurements at different age points. We estimated $\tilde{\rho}_l$ as the ratio of first-third visit ρ_l and first-second visit ρ_l. The ratio cancels the impact of measurement error. We divide $log(\tilde{\rho}_l)$ by the average age difference between the second and third visits to estimate $\tilde{\rho}_l$ between individuals with one year of age difference (see **Methods**).

We estimated Δh^2 and $\tilde{\rho}_l$ for 16 quantitative traits across 180K individuals in the UK Biobank (**Supplementary Table 2**); the sample size reflects a restriction to individuals of British ancestry with diagnostic records from both primary care data and hospital inpatient data, which we imposed to mitigate the impact of missing diagnoses. The quantitative traits in this study were selected following ref. [18] (**Methods**). We use *cross-sectional design* to estimate Δh^2, where we compare individuals with different ages at the baseline visit. We evaluate the impact of recruitment bias that can arise from a cross-sectional design in a secondary analysis. We use *longitudinal measurement* to estimate $\tilde{\rho}_l$, where we compare multiple measurements at different age points of the same individual.

We estimate Δh^2 for the estimated disease liability of 9 diseases (**Supplementary Table 3**). We use 36 quantitative traits (**Supplementary Table 4**) to estimate disease liability at baseline age by predicting binary disease phenotypes from the quantitative traits. We do not estimate $\widetilde{\rho_l}$ for estimated disease liability because we do not have longitudinal measurements for all quantitative traits that were used to estimate disease liability.

We study the impact of age-dependent disease architecture on disease prediction using simulations. We extract age-at-diagnosis for each patient using the first diagnosis in either primary care data or hospital inpatient data to evaluate age-dependent disease prediction accuracy in empirical data. We construct PRS and non-genetic predictors using five-fold cross validation without age stratification. We have publicly released summary data of age-specific heritability, phenotypic correlation, and genetic correlation estimates (see **Data Availability**). We have also released software to compute age-dependent heritability and prediction accuracy (and **Code Availability**).

Age-dependent genetic architecture of quantitative traits

We estimated Δh^2 w.r.t. age of 16 quantitative traits (**Supplementary Table 2**) to evaluate the evidence supporting the EA model. First, we found 5 of the 16 traits have significantly decreasing heritability with age (p<0.05/9, FEV1/FVC, LDL cholesterol, total cholesterol, diastolic blood pressure, and systolic blood pressure) with an average 10-year decrease of 17.8% in h^2 (**Figure 1A**, **Supplementary Table 5, Supplementary Figure 1**). Second, we computed genetic and environmental variance of each age quintile using heritability and phenotypic variance estimates (**Figure 1B, Supplementary Figure 2, Supplementary Figure 3, Supplementary Table 6, Supplementary Table 7**). We estimated phenotypic variance for males and females separately to account for sex differences[5,13], which provides estimates for 32 trait-sex pairs. We found $\Delta var(E)$ is significantly larger than $\Delta var(G)$ for 10 trait-sex pairs (red dots in **Figure 1B**), supporting the EA model. We found $var(E)$ and $var(G)$ vary proportionally with age in traits that do not have significant age-varying heritability (grey dots in **Figure 1B**), supporting a proportional amplification model that has been observed in GxE studies[5,13]. The EA model will move traits above the diagonal line in **Figure 1B**, while the proportional amplification model will move traits along the diagonal line. Taken together, we conclude that FEV1/FVC, LDL cholesterol, total cholesterol, systolic blood pressure, and diastolic blood pressure show evidence for the EA model.

Next, we estimated genetic and phenotypic correlations between age groups to evaluate additional evidence in support of the EA model. $\rho(G_{younger}, G_{older})$ is expected to equal 1.0 and $\rho(E_{younger}, E_{older})$ is expected to be less than 1.0 under the EA model. We found the genetic correlation, $\rho(G_{younger}, G_{older})$, was close to 1.0 for most traits, with exceptions of HbA1c (p=1e-4) and glucose (p=3e-4) (**Figure 2A, Supplementary Table 8**). A genetic correlation less

than 1.0 supports a model where genetic components have different age profiles (**Supplementary Table 1**), which is consistent with our previous work that showed that genetic variants have distinct age profiles in conveying common disease risk[4]. We computed the denoised phenotypic correlation $\widetilde{\rho_l}$ to evaluate the environmental correlation across age ($\rho(E_{younger}, E_{older})$) (**Methods**). For the 11 traits that have longitudinal data for 3 visits, 7 have $\widetilde{\rho_l}$ significantly less than 1.0 (**Figure 2B, Supplementary Table 9**), supporting the EA model. $\widetilde{\rho_l}$ has high correlation with Δh^2 w.r.t. age (ρ=0.61 across 11 traits, **Figure 2C**), which is consistent with the EA model. Specifically, the 3 traits (Systolic BP, Diastolic BP, and FEV1/FVC) that show evidence supporting the EA model in **Figure 1** have the largest difference between $\widetilde{\rho_l}$ and 1. Our analysis of the genetic and environmental correlation between young and old individuals provides orthogonal evidence in support of EA for systolic blood pressure, diastolic blood pressure, and FEV1/FVC.

We performed six secondary analyses to test the robustness of our results. First, we tested whether age-dependent recruitment bias of individuals with different health status could explain decreasing heritability estimates. We created two age-matched samples (mean age: 55.9 vs. 56.6) with high and low numbers of prevalent disease diagnoses (mean diagnoses: 6.8 vs 34.6) and estimated the heritability of 16 quantitative traits in the two groups. We observed minimal heritability differences between the two groups, which suggests that biased recruitment of healthier older individuals in the UK Biobank[19] does not contribute to the decreasing heritability estimates with age (**Supplementary Figure 4**). Second, we evaluated the amplification models[5,11] by estimating changes in genetic variance w.r.t. age for 32 trait-sex pairs (**Supplementary Figure 2, Supplementary Table 7**). We found 25 traits with age-varying genetic variance, align with previous GxSex and GxE studies that report amplifications[5,13]. Third, we tested an alternative model where exposure accumulation decays with age by identifying traits with Δh^2 close to zero but a denoised phenotypic correlation less than 1.0 across age bins. We found evidence support this model for BMI and body WHR among the traits that we can estimate $\widetilde{\rho_l}$ (i.e. those with multiple measurements) (**Supplementary Table 9**). Fourth, we tested a non-proportional amplification model by identifying traits with both genetic correlation and denoised phenotypic correlation close to 1 but age-varying heritability (**Supplementary Table 9**). We found no such traits among the traits that we can estimate $\widetilde{\rho_l}$. Fifth, we estimated genetic correlation between the top and bottom age quantiles (median age difference = 22.0) without meta-analyzing across age bins and found smaller $\rho\left(G_{young}, G_{old}\right)$ compared with the meta-analyzed results with larger standard errors (**Supplementary Figure 5**). Sixth, we tested whether using age in years instead of age quintiles can explain more variance in quantitative traits. We found age quintiles explains similar R^2 as age in years (**Supplementary Figure 6A**), suggesting age quintiles capture the majority of age-related variation while allowing us to use standard methods to compute heritability and genetic correlations. We found adding an additional age^2 covariate to the age in years explains more

quantitative trait variance (mean R^2= 0.024 across 16 traits) than the model with only linear age in years (mean R^2= 0.022 across 16 traits).

Taken together, these results support exposure accumulation as the primary driver of age-dependent architecture in quantitative traits.

Age-dependent genetic architecture of estimated disease liability

We next investigated whether the liability of 9 diseases (**Supplementary Table 3**) is consistent with the EA model. We estimated disease liability by applying LASSO[20] to 36 quantitative traits (**Supplementary Table 4**) measured at baseline and predicting disease status in the entire population (i.e. across all age bins). We use the value predicted by LASSO as estimated liability to approximate disease liability (**Methods**).

We hypothesized that estimated liability is highly correlated with the true disease liability at the baseline age, thus can be used to study the age-dependent architecture of disease liability. We confirmed that the estimated liability achieves high accuracy across nine diseases, with an average liability-scale correlation of 0.603 (s.d. = 0.206 across nine diseases, **Supplementary Table 10**) with case-control status. We applied the same methods as in the quantitative trait analysis to the estimated liabilities to estimate Δh^2 and $\rho(G_{younger}, G_{older})$. We validated that h^2 of estimated liability is similar to the liability-scale $h^2$of the respective diseases (**Supplementary Figure 7**). We found the heritability of the predicted liability significantly decreases for 5 of the 9 predicted disease liabilities (**Figure 3A**, **Supplementary Table 11**, mean Δh^2 = -18.1%±2.7% for every 10 years of age), which supports the EA model of disease liability. We observe genetic correlations across age bins ($\rho(G_{younger}, G_{older})$) are significantly different from 1 for coronary artery disease (CAD) and T2D (**Figure 3B**, **Supplementary Table 12**), which aligns with previous observations of heterogeneous age profiles in CAD[6] and subtypes of T2D[21–23]. Taken together, we determined the estimated liabilities of asthma, hypertension, high lipid, COPD, and high cholesterol follow the EA model.

Simulations implicate factors contributing to age-dependent disease PRS accuracy

We hypothesized that the following 3 factors could contribute to age-dependent disease PRS accuracy: (i) age-dependent liability under a liability threshold model[6,14]; (ii) prediction of incident cases (instead of prevalent cases)[24]; and (iii) exposure accumulation under our new EA model. We refer to these three hypotheses as factors (i) - (iii)

First, the intuition of factor (i) is that older cases have disease liability closer to healthy individuals compared to younger cases (see **Methods** and **Supplementary Note**). Under the liability-threshold model (**equation 1**), L increases as the population ages, which causes older

249 cases to have liability that is closer to the healthy controls compared to the cases that reached the
250 threshold at a younger age (**Figure 4A**, ref [16]**)**. Therefore, the difference between cases and
251 controls becomes smaller for the older population, which causes decreasing prediction accuracy.
252 In **Supplementary Note**, we show that the difference between the genetic values of cases and
253 controls strictly decreases with age, which aligns with the intuition that liability of older cases is
254 closer to healthy controls.
255
256 Second, the intuition of factor (ii) is that excluding prevalent cases at baseline will create
257 negative correlation between the predictable component and non-predictable component of
258 disease liability, which reduces prediction accuracy (see **Supplementary Note)**. We note that
259 there are two ways to define cases and controls at a specific age point (**Figure 4A**). First,
260 *prevalent case association* defines cases as individuals who are diagnosed with the disease
261 before the age point and controls as individuals who have not had a diagnosis of the disease at
262 least until the age point; prevalent case association is a common choice in constructing genetic
263 risk scores[18,25–28]. Second, *incident case prediction* defines cases as individuals who are
264 diagnosed for the first time within a time window after the age point and controls as individuals
265 who are not diagnosed at least until the end of the time window; incident case prediction is a
266 common choice in clinical risk prediction[29,30]. We report results from both case-control
267 definitions but focus on the latter because incident case prediction has more clinical utility.
268
269 Third, the intuition of factor (iii) is that PRS prediction accuracy decreases with age when
270 heritability decreases with age (see **Supplementary Note**). Under the proposed EA model,
271 heritability will decrease due to exposure accumulation, causing decreasing PRS accuracy with
272 age.
273
274 We performed simulations to evaluate the contribution of factors (i)-(iii) to age-dependent
275 prediction accuracy. Our simulation framework modeled liability increasing linearly with age.
276 The age of onset is determined when the liability of an individual reaches a fixed threshold. We
277 evaluate prediction accuracy using the observed R^2 with 1:1 case-control ratio ($R^2{}_{obs}$), area
278 under the ROC Curve (AUC), liability-scale R^2 ($R^2{}_{liab}$), and log odds ratio ($logOR$). Further
279 details are provided in the **Methods** section.
280
281 $R^2{}_{obs}$, AUC, and $logOR$ all decrease with age for both prevalent case association and incident
282 case prediction, while $R^2{}_{liab}$ decreases with age for incident case prediction but not for prevalent
283 case association, supporting the contribution of factor (i) to age-dependent prediction accuracy
284 (orange and purple curves in **Figure 4B; Supplementary Figure 8A**). Incident case prediction
285 accuracy decreases more than the prevalent case association accuracy, supporting the
286 contribution of factor (ii). We found that prediction accuracy under the EA model decreases
287 more than under linear liability-threshold model, supporting the contribution of factor (iii) (grey
288 curves in **Figure 4B)**. We estimated $R^2{}_{liab}$ under a normal distribution assumption[31] in empirical

289 data analyses. We evaluated the accuracy of this approximation using simulations and found it
290 was accurate (**Supplementary Figure 8B**).
291
292 We show in the **Supplementary Note** that the *relative* contribution of factor (i) to age-dependent
293 prediction accuracy depends on the $R^2{}_{liab}$ of the predictor to the underlying L. To validate this
294 hypothesis, we simulated predictors with varying $R^2{}_{liab}$ to the underlying L, representing a
295 perfect predictor ($R^2{}_{liab} = 99\%$), a strong predictor ($R^2{}_{liab} = 50\%$), a clinical score ($R^2{}_{liab} =$
296 20%), and a PRS ($R^2{}_{liab} = 5\%$). Prediction accuracy decreased more steeply with age for
297 weaker predictors, while the difference is negligible between the clinical risk score and PRS
298 (**Figure 4C, Supplementary Figure 8A**).
299
300 Our analyses show that prediction accuracy decreases with age under the liability-threshold
301 model (factor (i)) using both analytical results and simulations, while the decreasing slope is
302 steeper when predicting incident cases (factor (ii)), predicting phenotypes that follow the EA
303 model (factor (iii)), and the predictors have low overall $R^2{}_{liab}$.
304
305 *Age-dependent prediction accuracy of PRS is partially consistent with liability-threshold model*
306 *and prediction of incident diseases*
307
308 We next evaluated whether the age-dependent disease PRS accuracy is consistent with factor (i)
309 and (ii) in empirical data. We computed PRS using BOLT-REML with fivefold cross validation
310 for 9 diseases without age stratification. We divided the cases into age quintiles based on the
311 earliest diagnosis age of each patient and created sample sets with a 1:1 case-control ratio to
312 ensure each age bin has the same sample size and case-control ratio. We computed 4 metrics to
313 measure incident case prediction accuracy: log hazard ratio ($logHR$), log odds ratio ($logOR$), the
314 effect size of PRS in a linear regression on case-control status, and $R^2{}_{obs}$. We also compute
315 $R^2{}_{obs}$ for prevalent case association using the median age of each age quintile as the age index.
316 We report the change of the 4 metrics ($logHR$, $logOR$, linear regression effects, and $R^2{}_{obs}$) by
317 fitting a model where the metric changes linearly with age. Briefly, we test for non-zero changes
318 in each metric with a likelihood ratio test between the model with age term and a null model
319 where the metric is constant with age (**Methods**). We report the 10-year change of each metric
320 relative to the estimates in the entire population.
321
322 We found PRS accuracy decreases with age across all diseases we studied, consistent with factor
323 (i). We started by evaluating the $logHR$ of each PRS to account for censoring. We found that the
324 $logHR$ of each PRS significantly decreased with age for 6 of the 9 diseases ($p<0.05/9$, **Figure**
325 **5A**, **Supplementary Table 10**), which aligns with a previous study that used lead GWAS
326 associations and observed decreasing effect sizes with age[6]. On average, the $logHR$ of each PRS
327 in the oldest quintile was 51%±5% of the youngest quintile. For example, the $logHR$ of the PRS
328 for predicting hypertension was 0.39±0.01 for the youngest quintile of cases (median(age_{onset}) =

47.1) and 0.16±0.01 for the oldest quintile of cases (median(age_{onset}) = 72.2). The $logHR$ of the PRS for predicting T2D is 0.32±0.02 for the youngest quintile of cases (median(age_{onset}) = 47.7) and 0.22±0.02 for the oldest quintile of cases (median(age_{onset}) = 72.8). These observations were consistent across different prediction accuracy metrics of PRS ($R^2{}_{obs}$, $logOR$, and linear regression effects, **Supplementary Figure 9, Supplementary Figure 10,** and **Supplementary Table 13**). We focus on $R^2{}_{obs}$ in later sections because it is on the same scale as h^2. We found the average 10-year decrease for incident case prediction accuracy ($R^2{}_{obs}$) was greater than the 10-year decrease in accuracy for prevalent case association (**Figure 5B, Supplementary Table 14**), consistent with simulations of factor (ii) in **Figure 4B** (orange curves versus purple curves, respectively). For example, $R^2{}_{obs}$ for PRS predicting hypertension decreases 50.0%±1.7% every 10 years of age in incident case prediction and 26.8%±3.3% for prevalent case association. $R^2{}_{obs}$ for PRS predicting T2D decreases 25.1%±4.2% every 10 years of age in incident case prediction and no longer decreases for prevalent case association (slope= -2.9%±4.2% per 10 years). Our analyses indicate that PRS prediction accuracy generally decreases significantly with age.

Exposure accumulation substantially impacts age-dependent disease PRS accuracy

We next evaluated whether the liability-threshold model (factor (i)), for incident case prediction (factor (ii)), and the EA model (factor (iii)) can explain age-dependent disease PRS accuracy in empirical data. We focus on incident case prediction so that all reported age-dependent prediction accuracy contains the contribution of factor (ii). We create quantitative risk scores (QRS) using quantitative traits to predict diseases. Because quantitative traits contain both genetic and non-genetic information, QRS does not contain the impact of the EA model. Therefore, age-dependent QRS prediction accuracy represents the contribution from factor (i) and factor (ii). We used the same 36 baseline quantitative traits to create QRS for each disease and add Gaussian noise so that QRS and PRS have the same $R^2{}_{liab}$ in the entire population (**Methods**). We compute the proportion of observed decrease in PRS accuracy with age that can be explained by each model to evaluate the contribution of the factor (i)-(iii) (**Methods**).

We found the liability-threshold model (factor (i)) and EA models (factor (iii)) together explain the observed age-dependent prediction accuracy of PRS for incident case prediction (factor (ii)). First, under the liability-threshold model for incident case prediction (factor (i)+(ii)), predictors using genetic data and predictors using non-genetic data (*i.e.* measurements of quantitative traits and environmental exposures) are expected to have the same age-dependent prediction accuracy, if they explain the same amount of variance in the liability ($R^2{}_{liab}$) (**Figure 4C**). We used the change of QRS $R^2{}_{obs}$ with age to estimate the contribution from factor (i) + (ii) (**Methods**). We found 65.1%±11.3% of the change of PRS $R^2{}_{obs}$ with age are explained by these two factors (**Figure 6A**, **Supplementary Table 15** and **Supplementary Table 16**). The change of QRS $R^2{}_{obs}$ with age is significantly different from the change of PRS $R^2{}_{obs}$ with age for hypertension (p=6e-8), asthma (p = 9e-13), and CAD (p = 7e-7). We determined that factor (i) + (ii) explains

most, but not all of the decreasing PRS prediction accuracy. Second, under the EA model (factor (iii)), the heritability of disease liability decreases with age, which causes PRS (which only captures genetic variance) accuracy to decrease with age. We found Δh^2 of disease liability is not large enough to fully explain the decrease in PRS prediction accuracy (**Figure 6B**), suggesting the EA model in disease liability (factor (ii)) is insufficient to explain all of decreasing PRS prediction accuracy.

Lastly, we combine the effect of EA model with liability-threshold model by computing the product of QRS ${R^2}_{obs}$ and h^2 of predicted liability as the expected prediction accuracy of PRS, which captures the contribution of factors (i), (ii), and (iii). We determined that 85.8%±9.8% of the observed age profiles of PRS is explained by the factor (i)+(ii)+(iii) (**Figure 6C, Supplementary Table 17**). A model with factors (i)+(ii)+(iii) explains significantly more observed $\Delta {R^2}_{obs}(PRS)$ with age than the model without factor (iii) (p = 4e-6). We note that CAD cannot be explained by our models (p = 3e-7 for x and y difference in **Figure 6C**). CAD also has $\rho(G_{younger}, G_{older})$ < 1.0 (**Figure 3B**), suggesting that age-dependent genetic heterogeneity might cause the deviation from the liability-threshold + EA model. Taken together, our results suggest that the liability-threshold (factor (i)), incident case prediction (factor(ii)), and the EA model (factor (iii)) explain age-dependent prediction accuracy of PRS.

Age-dependent accuracy of non-genetic predictors of disease

We investigated whether the liability-threshold model applies to age-dependent accuracy of both genetic and non-genetic predictors. We constructed risk predictors using the 36 quantitative measurements as non-genetic variables to further validate the liability-threshold model as a general model of disease. We note these 36 quantitative measurements contain both genetic and non-genetic (but predominantly non-genetic), but we use "non-genetic" to distinguish from analysis that focus on G. For each disease, we constructed 4 predictors with varying prediction power: (1) "QRS" predictor which is a LASSO predictor that uses all 36 quantitative measurements, (2) A "Top 3" predictor that is a joint linear predictor trained using the top three variables ranked by the ${R^2}_{liab}$ with target disease, (3) "single (strong)" predictors which are the quantitative measurements that rank 1st-3rd by the ${R^2}_{liab}$ with target disease, (4) "single (weak)" predictors which are the quantitative measurements that rank 4th and 5th. We trained all predictors using five-fold cross validation and estimated their prediction accuracy of diseases in each age quintile based on baseline UK Biobank visit. We then computed the change of ${R^2}_{obs}$ w.r.t. age for each predictor using the same method as the previous sections.

Predictors with greater prediction power in the entire population have less age-dependent prediction accuracy (**Figure 7A**, **Supplementary Table 18,** and **Supplementary Table 19**), as predicted by simulation results (**Figure 4C, Supplementary Note**). Relative change of R^2_{obs} w.r.t. age is -47.6%±1.3% for "single (weak)" predictors (avg(${R^2}_{liab}$) = 9.8%) and -23.6%±1.1%

for "QRS" predictors (avg($R^2{}_{liab}$) = 32.3%), averaging across the 9 diseases. We further expand to 10 predictors for each disease (QRS, "Top 3", each of the top 5 predictors, "top 2", PRS, PRS + QRS, restricting to predictors with $R^2{}_{liab}$ > 5% for adequate power) and found strong positive correlations between relative change of R^2_{obs} w.r.t. age and $R^2{}_{liab}$ across disease-predictor pairs (**Figure 7B**, slope = 0.64, p =1.2e-5). We conclude that predictors that use environment variables have decreasing accuracy with age and the effect is stronger for predictors with low overall prediction accuracy, suggesting combining genetic and non-genetic predictors can increase prediction power in older populations.

Discussion

We systematically quantified age-profiles of genetic and environmental variation to understand how complex disease architecture and polygenic risk score (PRS) accuracy vary with age. We found exposure accumulation is common in quantitative traits and complex diseases. We found the age-dependent PRS accuracy can be explained by a combination of a liability-threshold model and the exposure accumulation model. Our analysis was enabled by a novel approach to study estimated disease liability. Finally, we found both genetic and non-genetic predictors decrease in prediction accuracy with age in empirical data and simulations.

Our study represents an advance over previous studies that investigate age-dependent effects. First, we identify changes in genetic and environmental variance across 16 complex quantitative traits and 9 diseases. While previous work has studied age-dependent effects, they have focused on single variant effects[32] or have studied a limited set of phenotypes[12,13,33–39]. Second, to the best of our knowledge, our work is the first to quantify how environmental variance in complex traits accumulates with age using longitudinal data. Third, our work is the first to provide a quantitative explanation for the decrease in prediction accuracy for genetic and non-genetic predictors. While other studies have observed this phenomenon, they have not been able to explain it[6,11]. We note, however, that CAD was an exception to the EA model and, while we speculate that this may be due to age-dependent genetic heterogeneity, this is something of a mystery to be resolved in subsequent studies. Lastly, our work demonstrates that PRS trained and tested using prevalent case association[18,25–28] shows different age-dependent accuracy compared with incident case prediction, underscoring the importance of evaluating PRS accuracy using incident case prediction, which has greater clinical utility[32–35].

Our study has several implications. First, the EA model suggest GWAS study can increase power by accounting for age-dependent heritability. In particular, we hypothesize that mixed effect model can increase power by modelling age-specific random effects. Second, the EA model suggests when incorporating PRS in clinical risk models, PRS should be weighted differently with age to increase power. Third, our results suggest all predictors (*i.e.* genetic or non-genetic) of disease have age-dependent accuracy, while predictors with stronger prediction power in the

entire population will have more robust prediction accuracy at older age. This motivates constructing predictors that combine multiple data modalities to achieve maximal prediction accuracy across age. Fourth, the observed exposure accumulation suggests genetic effects contribute more to phenotypic variation at early ages, suggesting ascertaining environment variables is critical to accurately predict phenotypes at later ages. Lastly, our results suggest recruiting younger cases can improve power for discovering both genetic and environment biomarkers for diseases. All of these implications motivate directions for future research.

Our study has several limitations. First, our modeling is not able to detect uniformly decreasing genetic variance which can cause decreasing h^2 with age and $\rho\left(G_{young}, G_{old}\right)$ close to 1. However, we believe this is not likely because we found evidence of accumulating environmental variance in the $\widetilde{\rho_l}$ analyses which explains the decreasing h^2 (**Figure 2C**). Second, the age range of our study sample is restricted, with baseline visit age between 40 to 79 years of age. Future analyses with a wider age distribution may discover stronger effects. Third, we use a cross-sectional analysis, which is susceptible to recruitment bias. We tested whether age-dependent recruitment bias of healthier individuals could explain decreasing heritability estimates with age and observed minimal heritability differences between the two groups, suggesting a minimal effect of biased recruitment. Fourth, our analyses uses only individuals of European individuals. While it is of interest to perform the analysis on individuals of other ancestries, currently available data of other genetic ancestry might not have sufficient power for age-stratified analyses. Fifth, our analyses use the UK Biobank data set. It is of interest to replicate the analysis in other cohorts such as All of Us[36]. Sixth, majority of our findings rely on the validity of liability-threshold model, although liability-threshold model has been widely accepted and used[14,15,37–43]. Despite these limitations, our work identifies exposure accumulation as a key aspect age-dependent disease architecture, and our results explain the decreasing genetic and non-genetic disease prediction accuracy with age.

Methods

Study population in UK Biobank

We used the disease diagnosis information from 180,026 individuals whose primary care data (General Practice, GP) was available and of British Isle ancestry. The primary care data are coded in readv2 which were mapped to SNOMED CT (https://digital.nhs.uk/services/terminology-and-classifications/read-codes), SNOMED CT codes were then mapped to ICD-10 codes (using NHS digital's code mapping https://digital.nhs.uk/), which were combined with ICD-10 codes from Hospital Episode Statistics (HES) and mapped to PheCodes [44]. We extracted the earliest diagnosis age using the earliest records from the combined primary care and HES data, which are used as age labels in our analysis. The choice of focusing on individuals with both primary data and HES data was to get the best age at diagnosis for each disease. When combining GP and HES data to extract diagnosis, correlation between binary and quantitative traits increased compared to only using HES data to extract disease

489 (**Supplementary Figure 11**), suggesting that combining GP and HES data capture diagnoses
490 more accurately as correlation decreases when variables are measured with noise.
491
492 Selection of quantitative and binary traits
493 We extracted 36 quantitative traits measured at baseline visit of UK Biobank based on ref. [18]. As
494 our goal is to study disease liability, we selected 9 diseases using phecodes that have
495 interpretable underlying quantitative traits from the 36 quantitative traits (e.g. Hb1Ac for T2D,
496 BMI for obesity, LDLc for hypercholesterolemia) and prevalence higher than 5%
497 (**Supplementary Table 3**). Disease status and age-at-diagnosis were extracted from GP+HES
498 data described in the previous section.
499
500 We corrected blood biochemistry measurement for cholesterol, hypertensive, and diabetic
501 medications: cholesterol (+1 s.d.), LDL-c (+ 1 s.d.), and triglyceride levels (+0.5 s.d.) were
502 corrected for lipid lowering medication[45]; systolic blood pressure (+15 mm Hg) and diastolic
503 blood pressure (+ 10 mm Hg) were corrected for hypertension medication[46]; HbA1c level is
504 corrected for non-insulin diabetic medication (+ 10.929) and insulin drugs (+ 1.3 x 10.929)[47].
505 The respective changes for individuals who are taking the medication are in the parentheses after
506 each trait; s.d. is the standard deviation computed in the entire population. We verified that the
507 correlation between the corrected quantitative traits and corresponding binary traits is higher
508 compared to the correlation between uncorrected quantitative traits and the same set of binary
509 traits. $\rho(LDL, hypercholesterolemia)$: 0.188 post-medication correction vs -0.005 pre-
510 correction. $\rho(Systolic\ blood\ pressure, hypertension)$: 0.519 post-medication correction vs
511 0.425 pre-correction. $\rho(HbA1c, T2D)$: 0.565 post-medication correction vs 0.524 pre-correction.
512 Both corrected and uncorrected values were included in the final 36 quantitative traits.
513
514 In our analyses, smoking status is defined as an ordinal variable with the following values: never
515 (0), previous (1), current (2) (**Supplementary Table 4**).
516
517 To select quantitative traits that are most relevant to the nine diseases, we further computed the
518 correlation between the 36 quantitative traits and the nine disease traits and selected 16 of the 36
519 quantitative traits based on liability-scale correlation [31]; the included quantitative traits are
520 among the top 3 correlated traits for at least one of the nine binary diseases.
521
522 Heritability and genetic correlation
523 We estimated heritability using the REML function of BOLT-LMM[17] version 2.4.1. 180,026
524 individuals were divided into 5 age bins based on the baseline visit age. We performed REML
525 analysis for each age bin using sex and baseline visit age as covariates; we use the same 536,492
526 HapMap3 SNPs that have moderate LD with each other which is the same as the PRS section,
527 see below. We also computed the heritability of 16 quantitative traits and nine diseases in the
528 entire population.

We estimated genetic correlation between age bins for the 16 quantitative traits using LDscore regression[48]. First, we used the mixed-effect model to compute summary statistics for each age bin using BOLT-LMM version 2.4.1. We used the same set of variants and individuals as the heritability estimation. Since BOLT-LMM is a mixed effect model that controls population stratification, we constrained the heritability intercept of LDSC to 1.0; we constrained covariance intercept to be 0 as there is no sample overlap between different age bins. We run cross-trait LDSC for each age-bin pair (10 pairs in total for 5 age bins) to estimate the genetic correlation and its standard error.

Testing for heritability changes across age bins

We tested the age-dependency of heritability using heritability estimates with standard error across the five age bins. We used likelihood ratio tests to identify non-constant heritability across age bins. We tested two nested models: H_0: $h^2 \sim N(0 \times age + b, s.e.(h^2))$ and H_1: $h^2 \sim N(a \times age + b, s.e.(h^2))$. We estimated b under H_0 and a, b under H_1 using maximum likelihood estimators across the five heritability estimates. For each age quintile, we use the median age to fit the model. The slope a estimated under H_1 are the per year change of h^2. We use Monte-Carlo sampling of h^2 for each age quintile from a Gaussian distribution with mean equals to the point estimates and variance equals to s.e.. We estimate a, b of each Monte-Carlo sample. The s.d. of a estimates across Monte-Carlo samples are the s.e. of the estimates. We note this approach relies on the fact that samples are non overlapping across age quintiles.

In all analyses, we report the relative change of heritability compared to the heritability estimate in the entire population.

Testing for genetic correlation less than 1 between age bins

The quantity of interest is the difference between genetic correlation and 1: $1 - \rho_g$. First, we scale genetic correlation using $\rho_{normalised} = exp(10 \times ln\, \rho_{\Delta age} / \Delta age)$ to account for the varying age differences of age-bin pairs; the age differences are computed using the median of each age quintile. Scaling on the exponential scale aligns with a Wiener process of liability w.r.t age (see below). For 5 age bins, we can estimate 10 genetic correlations between pairs of age bins; these 10 genetic correlations have four degrees of freedom. Therefore, we use inverse-variance weighting to meta-analyse four of the 10 scaled ρ_g (we use ρ_g of neighboring age-bin pairs 1-2, 2-3, 3-4, and 4-5) to compute one 10-year r_g for each trait; standard errors of the 10-year r_g estimates are used for inverse-variance weights.

Computing phenotypic correlation across age points

Under the assumption that random variance accumulates linearly w.r.t. age (as in a Wiener process), the correlation between liability across age bins is a function on the multiplicity scale

568 $\rho_{\Delta age} = e^{-\beta\, \Delta age}$. Therefore, we computed the expected 10-year genetic and phenotypic
569 correlation by $exp(10 \times ln\, \rho_{\Delta age} / \Delta age)$ to make the correlations comparable for age bin pairs
570 with different age differences. We computed phenotype correlations across individuals who have
571 three visits to the UK Biobank. We remove the impact of measurement error by computing a
572 ratio of two correlations $\rho_{\Delta age} = \rho_l(t_1, t_3)/\rho_l\,(t_1, t_2)$, which cancels out the measurement
573 error, and we use the average age difference between second and third visit ($\Delta age = t_3 - t_2$) to
574 scale the estimate.
575
576 Testing the impact of selection in recruitment process
577 To test for whether the age-dependent heritability changes can be attributed to selected
578 recruitment of healthier individuals at older age groups[19], we computed the number of past
579 diagnosis records as an indicator of health status and created samples with matched age but
580 different past diagnosis. We used health records from both GP and HES, and divided the target
581 population into two groups, "healthy" versus "unhealthy", using the median number of prevalent
582 records (median=16). We then use inverse probability weights to sample 45,267 individuals from
583 both groups, resulting in two samples that have matched age distributions (mean: 55.9 vs. 56.6,
584 respectively) but different numbers of past diseases (mean: 6.8 vs 34.6, respectively); in
585 comparison, top and bottom age quintile has an average age of 67.5 and 45.3 and an average of
586 24.2 and 18.7 of past diseases, respectively. We compute heritability of the 16 quantitative for
587 both groups using the same procedure as for age quintiles.
588
589 PRS construction
590 We obtained 536,492 HapMap3 SNPs using pruning parameters of window size=50 kb, step
591 size=5 kb, and r^2 threshold=0.8; selection of SNPs makes mixed effect model computational
592 tractable. We then used BOLT-LMM to estimate PRS, using genetic sex and age at baseline as
593 covariates, using 5-fold cross validation for the 9 diseases and 16 quantitative traits. PRS are
594 scaled to have mean=0 and sd=1 in the entire population.
595
596 PRS incident case prediction and prevalent case association
597 For incident case prediction, we first divided cases into five age quintiles based on their first age-
598 at-diagnosis; for each age quintile, we define case control status based using interval-censor
599 procedure [6], where cases are defined as those who are diagnosed within the age interval and
600 controls are defined as those who remained healthy till the end of age interval or lost to follow up
601 within the age interval. We then down sampled the controls for each age bin to have the same
602 number as the cases. As a result, for a given disease, each age interval has exactly the same
603 number of cases and controls which ensures the odds ratio and hazard ratio are comparable
604 across each age bin. When evaluating PRS using linear, logistic, and Cox regression models, we
605 included genetic sex and top five genetic PCs as covariates. When evaluating PRS using
606 observed-scale R^2, we first regress the outcome on genetic sex and top five genetic PCs, then

compute Pearson's correlation between the residual and PRS; the square of Pearson's correlation is the observed-scale R^2 with 1:1 case control ratio.

For prevalent cases association, we used the five median case age of the respective age intervals as the baseline age points and considered all individuals who have been followed up past the baseline age point. The prevalence cases are defined as those who have at least one diagnosis record before the baseline age point. We sampled controls to be the same number as cases for each age point, so that for a given disease, the effect sizes of linear, logistic, and Cox regression across five baseline age points are comparable. The regression models and observed-scale R^2 were computed using the same covariates as in incident case association.

Estimated disease liability

We use 36 continuous traits measured at baseline to predict the 9 binary disease traits; the resulting predictor is the *estimated disease liability*. Cases are defined as the union of both incident and prevalent disease. We use LASSO linear model (instead of logistic regression as we assume a liability-threshold model) to train the prediction models with 10-fold cross validation; the regularization coefficients are chosen by the cross-validation with both 1se (default setting of the R glmnet package[49,50]) and 2se (stronger regularization). We chose the predicted liability using the 2se model as it has a similar liability-scale correlation (average=0.60 across 9 diseases) with the binary trait to the 1se model (average=0.61 across 9 diseases), while being more explainable and less susceptible to overfitting. The models were fitted in the entire population without including age as a covariate so that the predicted disease liability represents the approximate disease liability at the age of baseline visit.

We used the same procedure as the quantitative traits analysis to estimate heritability and genetic correlation for predicted liability. We used BOLT-REML to estimate heritability. We used BOLT-LMM to compute GWAS summary statistics then use cross-trait LDSC to estimate genetic correlation of each age-bin pair (10 pairs in total for 5 age bins) to estimate the genetic correlation and its standard error. We did not constrain intercepts for cross-trait LDSC to avoid potential bias population relatedness.

Simulation of linear liability-threshold model

We simulated genetic variance G and environment variance E from normal distribution with mean 0 and variance equal to h^2 and $(1-h^2)$ respectively. Liability L equals the sum of G and E for each individual. To simulate liability increasing with age, we take 2% of the simulated individuals with the highest liability as the youngest disease group, top 2-4% of liability as the second age group and repeated the procedure to obtain five groups of individuals with increasing onset age. Each disease threshold corresponds to the disease cut off at an age point. Prevalent cases are defined as the individuals that have liabilities higher than the threshold at a specific age point; incident cases are defined as individuals in the bin near the liability threshold at a specific

age point (i.e. all individuals with liability near the corresponding liability); controls are defined as all individuals excluding prevalent cases (i.e. all individuals have liability lower than the corresponding liability).We simulated 100,000 individuals, with h^2=0.3 and using five age bins of 2% of individuals, which matches the disease prevalence and sample size in empirical analyses.

We note our simulation uses percentiles of individuals to represent cases with increasing age, which aligns with the empirical analysis (see below) where we divided cases into quintiles based on the diagnosis age. We note under the proportional amplifciation model, the liability percentile of each individual does not change, which means this model is invariant to proportional amplification.

Simulation of EA liability-threshold model

We simulated initial liability L using the same procedure as the linear liability-threshold model. For each age bin, we sample cumulative environmental variance E_a from normal distribution with 0 mean and 0.05 variance. We then cumulatively add these sampled environmental variances to the liability when moving to an older age quintile, which will result in 20% more accumulated variance in the fifth age quintile. In empirical data, we found ~20% decrease in heritability over 20 years for quantitative traits, which motivates our choice of simulation parameters.

We defined prevalent cases as individuals who have got disease at any prior age bin or the current age bin, and incident cases as those who get disease within the current age bin. For each age bin, we take the top 2% individuals who have not prevalent diseases to simulate that liability increases with age. We note this simulation procedure makes the number of cases equal to previous simulation of the linear model so the metrics in **Figure 4B** are comparable.

Estimating age-dependent prediction accuracy under the linear liability-threshold model

We use rank normal transformation of estimated liability to create a *quantitative risk score (QRS)*. QRS combines both G and E information which is different from PRS that only captures G information; under the linear liability-threshold model, QRS and PRS has the sample age-dependent prediction accuracy profile when their liability-scale R^2 are equivalent across the population (**Figure 4C**). We performed the following 6 steps to use QRS to estimate expected age-dependency of PRS under the liability-threshold model. (1) QRS are rank normal transformed to have similar distributions as PRS. (2) QRS are adjusted for age at measurement and genetic sex; PRS are adjusted for first 5 genetic PCs and genetic sex. Adjustment of covariates ensures QRS and PRS are comparable under the linear liability-threshold model for each age bin, as QRS will change with age while PRS does not change with age. (3) We computed the liability-scale R^2 of QRS and PRS using all individuals with primary care information (N = 215,162); cases are defined as the union of prevalent cases and incident cases.

We computed observed-scale R^2 for both QRS and PRS and transformed observed-scale R^2 to liability-scale R^2 using equation 14 of ref [31]. (4) We added gaussian noise (mean = 0) to QRS so that the new QRS has the same liability-scale R^2 as PRS. (5) We computed QRS observed-scale R^2 for each age bin using the same case-control definition as incident case prediction of PRS. We note a caveat that some QRS are measured after disease diagnosis. Our choice is based on two reasons: first, under the linear liability-threshold model, QRS (age and sex adjusted) represents the liability that remains constant across age; second, observed-scale R^2 for QRS and PRS are computed using the same samples, making them comparable. We use QRS to predict incident cases at baseline visit and found similar results, see sections pertains to "non-genetic predictors". (6) We performed Monte-Carlo sampling to account for two sources of uncertainty: (i) the process to add noise to QRS and (ii) control sampling within each age bin. We reported mean and standard deviation of 50 Monte-Carlo sampling estimates for each parameter.

We define the proportion of observed decrease in PRS accuracy explained by each model as:

$$\tau = \sum_{diseases} \max(\Delta R^2_{QRS}, \Delta R^2_{PRS}) / \sum_{diseases} \Delta R^2_{PRS}.$$

The max in the numerator reflects the constraint that the proportion of age-dependent PRS accuracy that can be explained is less than 100%. Therefore, diseases with more decrease in QRS accuracy than PRS accuracy are assigned the same value in numerator and denominator. This choice is justified by empirical data as we do not observe significantly more decrease in QRS accuracy than PRS accuracy at a nominal *p*-value of 0.05, except for CAD.

<u>Estimating age-dependent prediction accuracy under the EA + liability-threshold model</u>

We multiplied the estimated slope from QRS with the slope of h^2 of predicted liability to estimate the expected decrease under the EA + liability-threshold model. Under the EA model PRS prediction accuracy is proportional to h^2 of disease liability at each age point. The EA + liability-threshold model estimates capture both the age-dependency from the linear liability-threshold model (captured by QRS) and the EA model (captured by the Δh^2 of predicted liability). The expected change is computed as 1 - $(1 + \Delta R^2{}_{QRS}) \times (1 + \Delta h^2{}_{predicted-liability})$. We use Monte-Carlo sampling of $\Delta R^2{}_{QRS}$ and $\Delta h^2{}_{predicted-liability}$ to estimate the standard error of the estimator; we omit the sampling covariance between $\Delta R^2{}_{QRS}$ and $\Delta h^2{}_{predicted-liability}$ as they were estimated from approximately independent information (*i.e.* $\Delta R^2{}_{QRS}$ were estimated using age quintiles of cases and baseline measurements, while $\Delta h^2{}_{predicted-liability}$ uses genetic information).

<u>Incident case prediction with non-genetic predictors</u>

For environment variable predictors, we divided incident cases into five age bins using the age at first diagnosis visit. We note that in contrast to PRS prediction accuracy, we excluded individuals who have prevalent cases before baseline visits as environment variables are measured at baseline visit. The definition of incident cases and controls for each age quintile, down sampling of control is the same as the PRS incident case prediction. We computed

727 observed-scale R^2 for each environment predictor by regression of sex and top five genetic PCs
728 from the outcomes and computed Pearson's correlation between the outcome residual and the
729 predictor; the square of Pearson's correlation is the observed-scale R^2 with 1:1 case control ratio.
730
731 We analyzed 10 predictors including 9 environment predictors and PRS. We computed the
732 relative change of observed-scale R^2 compared to the observed-scale R^2 estimate in the entire
733 population. Observed-scale R^2 in the entire population were transformed to liability-scale R^2
734 using equation 14 of ref [31]. When computing the relationship between liability-scale R^2 (in the
735 entire population) to the change of observed-scale R^2, we only include 61 of 90 predictors that
736 have liability-scale R^2 larger than 5% to ensure there is sufficient power to detect age-
737 dependency.
738
739 **Code Availability**
740 Code to replicate all analyses in the manuscript is available at https://github.com/Xilin-
741 Jiang/GxAge
742
743 **Data Availability**
744 Summary data in the manuscript is available at https://github.com/Xilin-Jiang/GxAge
745
746 **Acknowledgements**
747 Use of the UK Biobank data was performed under application number 7439. This research was
748 funded by Wellcome Trust early-career award 227566/Z/23/Z (X.J.) and the National Institute Of
749 General Medical Sciences of the National Institutes of Health under Award Number
750 R35GM16046 (A.D.). M.I. is supported by the Munz Chair of Cardiovascular Prediction
751 and Prevention and the NIHR Cambridge Biomedical Research Centre (NIHR203312) as well as
752 by the UK Economic and Social Research 878 Council (ES/T013192/1). J.D. is supported by a
753 British Heart Foundation Personal Chair. This work was supported by core funding from the
754 British Heart Foundation (RG/F/23/110103), NIHR Cambridge Biomedical Research Centre
755 (NIHR203312), BHF Chair Award (CH/12/2/29428), Cambridge BHF Centre of Research
756 Excellence (RE/24/130011) and by Health Data Research UK, which is funded by the UK
757 Medical Research Council, Engineering and Physical Sciences Research Council, Economic and
758 Social Research Council, Department of Health and Social Care (England), Chief Scientist
759 Office of the Scottish Government Health and Social Care Directorates, Health and Social Care
760 Research and Development Division (Welsh Government), Public Health Agency (Northern
761 Ireland), British Heart Foundation and the Wellcome Trust. The views expressed are those of the
762 authors and not necessarily those of the NIHR, the Department of Health and Social Care, or the
763 National Institutes of Health.

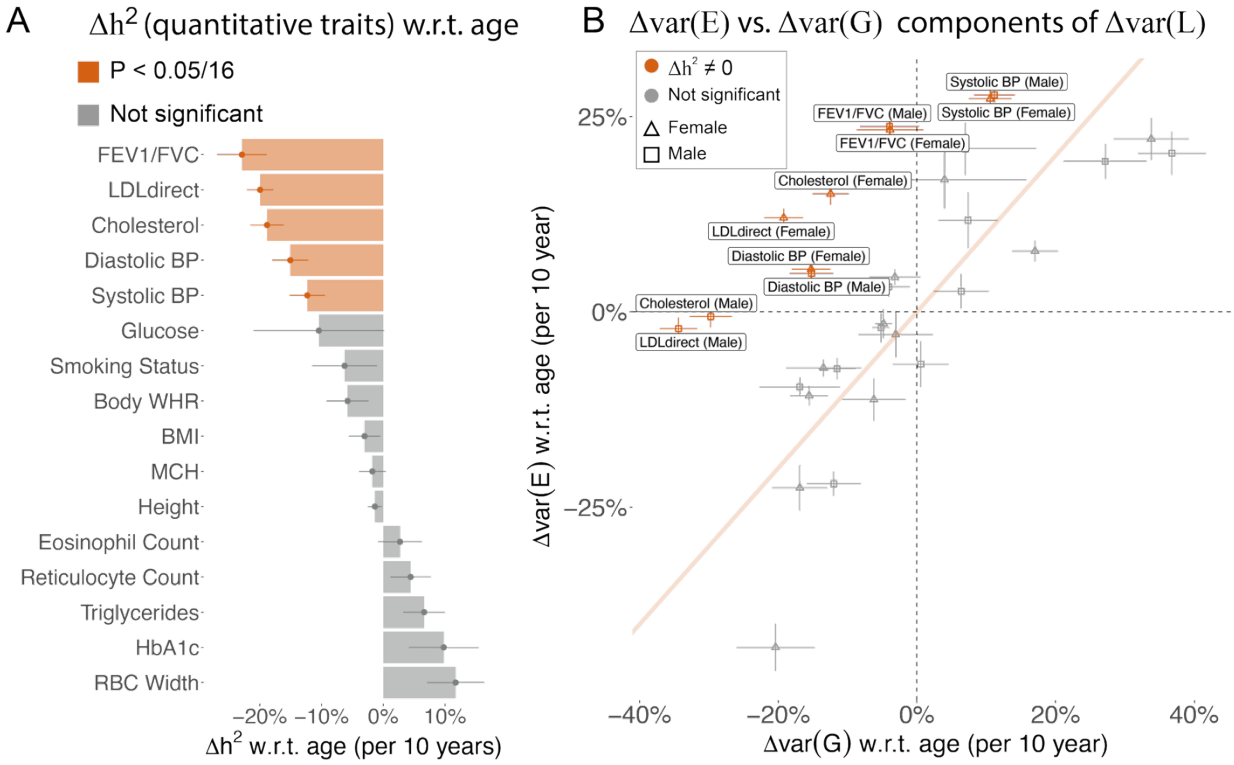

Figure 1. Age-dependent variance of quantitative traits. (A) Heritability changes per 10-years for 16 quantitative traits. Red bars show significant heritability changes across age; error bars show standard error via Monte-Carlo sampling. (B) 10-year change for genetic and environment variance for the 16 quantitative traits. Traits with significant age-dependent heritability are highlighted in red. Traits in grey show evidence of proportional amplification of genetic and environmental variance. Error bars are standard error via Monte-Carlo sampling. Numerical results are provided in **Supplementary Table 5 and Supplementary Table 7**. We note that no estimates are significantly outside the plausible range and that allowing estimates outside of the plausible range is necessary to ensure unbiasedness of estimates.

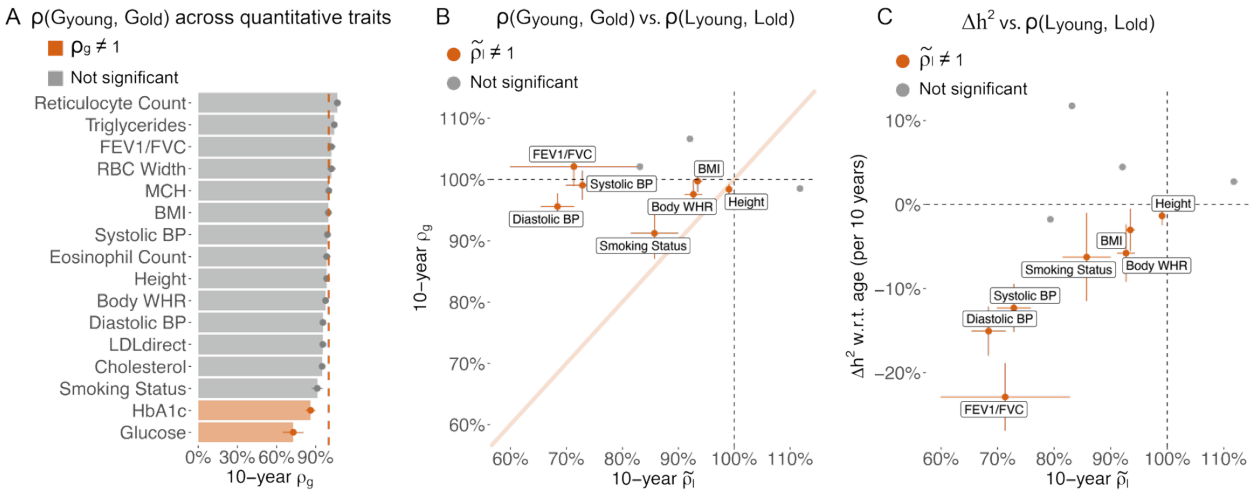

Figure 2. Genetic liability is more correlated across young and older age groups than environmental liability. (A) 10-year genetic correlation between younger and older age bins for 16 quantitative traits. We report the genetic correlation per 10-year age difference. (B) Scatter plot of 10-year genetic correlation versus denoised 10-year phenotypic correlation for the 11 quantitative traits that have three measurements per individual. We found no genetic correlation or phenotypic correlation that are significantly higher than 1 at nominal *p*-value = 0.05. (C) Scatter plot of heritability changes per 10-years versus denoised 10-year phenotypic correlation for the 11 quantitative traits that have three measurements per individual. Traits with denoised 10-year phenotypic correlation significantly different from 1 are shown in red and labeled in panel B and C; non-significant traits are shown in grey. Error bars for phenotypic correlation are standard error via bootstrapping over individuals; error bars for genetic correlation are standard error after meta-analysis across 4 age-bin pairs. Numerical results are provided in **Supplementary Table 8-9**. We note that no estimates are significantly outside the plausible range and that allowing estimates outside of the plausible range is necessary to ensure unbiasedness of estimates.

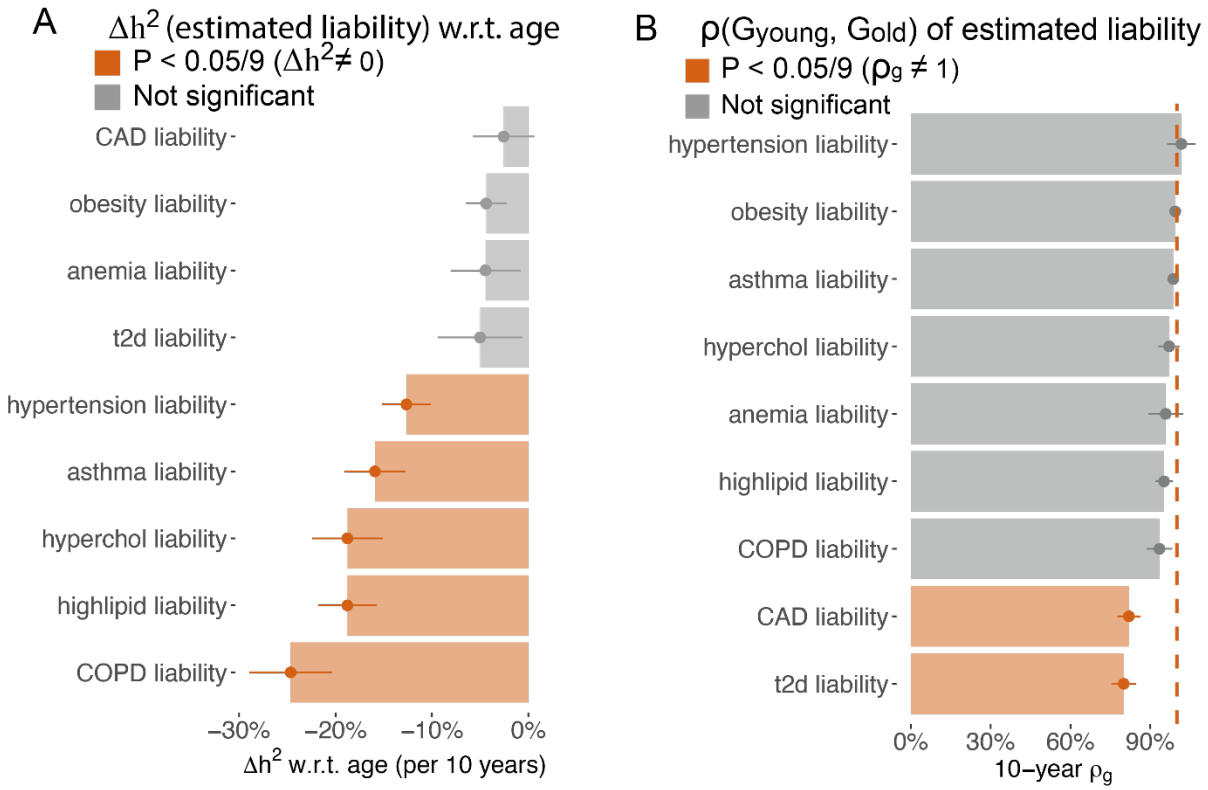

Figure 3. Age-dependent genetic architecture of estimated liability supports the EA model. (A) 10-year heritability change for estimated liability of 9 diseases; error bars show standard error via Monte-Carlo sampling. (B) 10-year genetic correlation for the estimated liability of 9 diseases. Error bars are standard error via meta-analysis of 10 age bin pairs. Numerical results are provided in **Supplementary Table 11-12**.

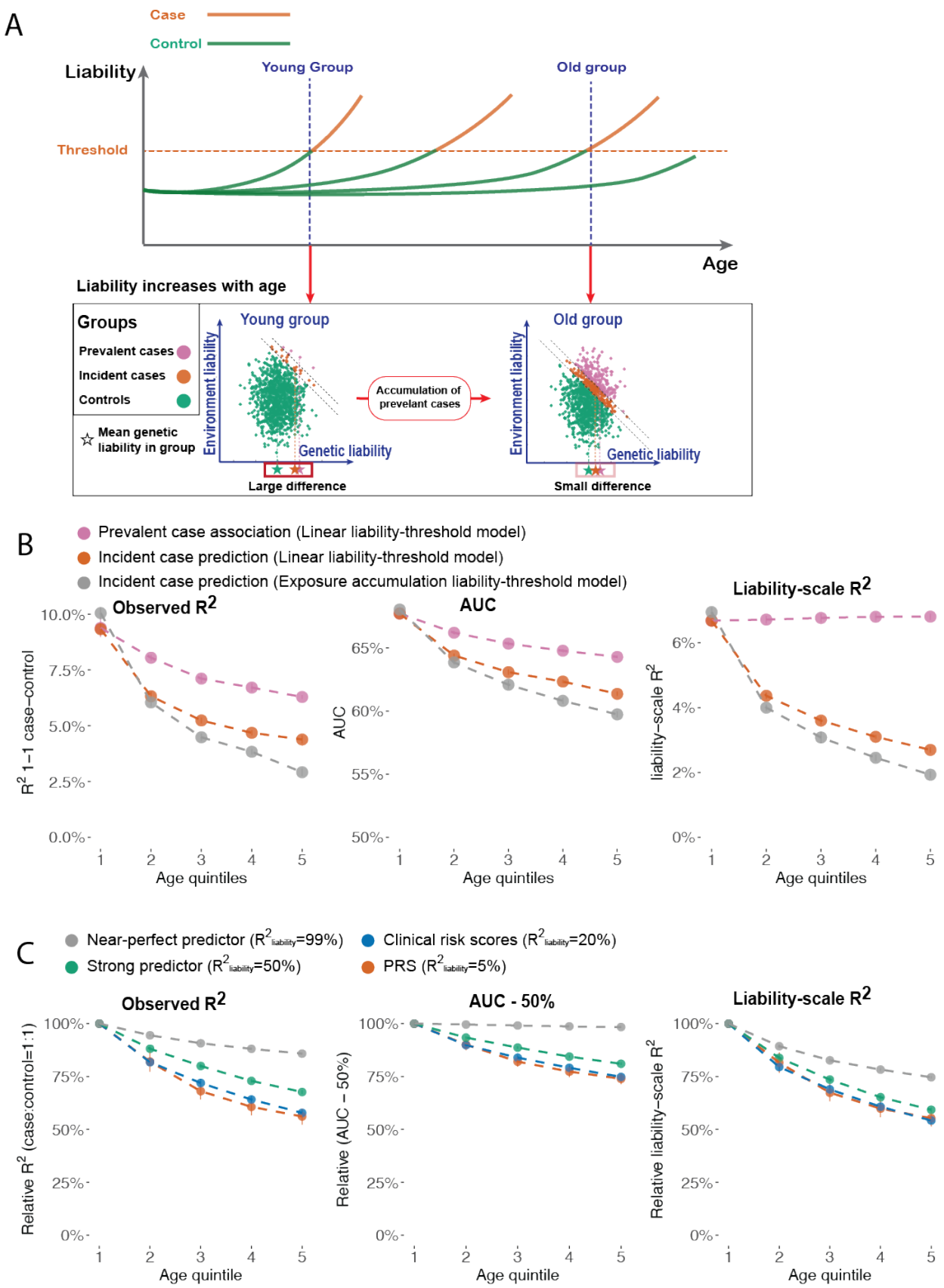
A
Case
Control
Liability
Young Group
Old group
Threshold
Age
Liability increases with age
Groups
Prevalent cases
Incident cases
Controls
Mean genetic liability in group
Young group
Environment liability
Genetic liability
Large difference
Accumulation of prevelant cases
Old group
Environment liability
Genetic liability
Small difference
B
Prevalent case association (Linear liability-threshold model)
Incident case prediction (Linear liability-threshold model)
Incident case prediction (Exposure accumulation liability-threshold model)
Observed R2
R2 1–1 case–control
10.0%
7.5%
5.0%
2.5%
0.0%
Age quintiles
AUC
AUC
65%
60%
55%
50%
Age quintiles
Liability-scale R2
liability–scale R2
6%
4%
2%
0%
Age quintiles
C
Near-perfect predictor (R2liability=99%)
Clinical risk scores (R2liability=20%)
Strong predictor (R2liability=50%)
PRS (R2liability=5%)
Observed R2
Relative R2 (case:control=1:1)
100%
75%
50%
25%
0%
Age quintile
AUC - 50%
Relative (AUC – 50%)
Age quintile
Liability-scale R2
Relative liability–scale R2
Age quintile

805

806 **Figure 4. Liability-threshold model and the EA model explains age-dependent disease**
807 **prediction accuracy in simulations.** (A) Schematic figure explaining the decreasing disease
808 prediction accuracy with age. In the top panel, each line represents the liability trajectory of an
809 individual. The panel below shows the joint distribution of genetic and environmental liability at
810 two age points. At later age points, cases are more similar to controls compared to earlier age
811 points. (B) Prevalent case association accuracy (purple), incident case prediction accuracy (red),
812 and Incident case prediction under the EA model (grey) across different age quintiles of cases.
813 Prediction accuracy is measured by observed-scale R^2 in 1:1 case-control matched samples,
814 AUC, and liability scale R^2 (C) Incident case prediction accuracy of predictors with different
815 liability-scale R^2.
816

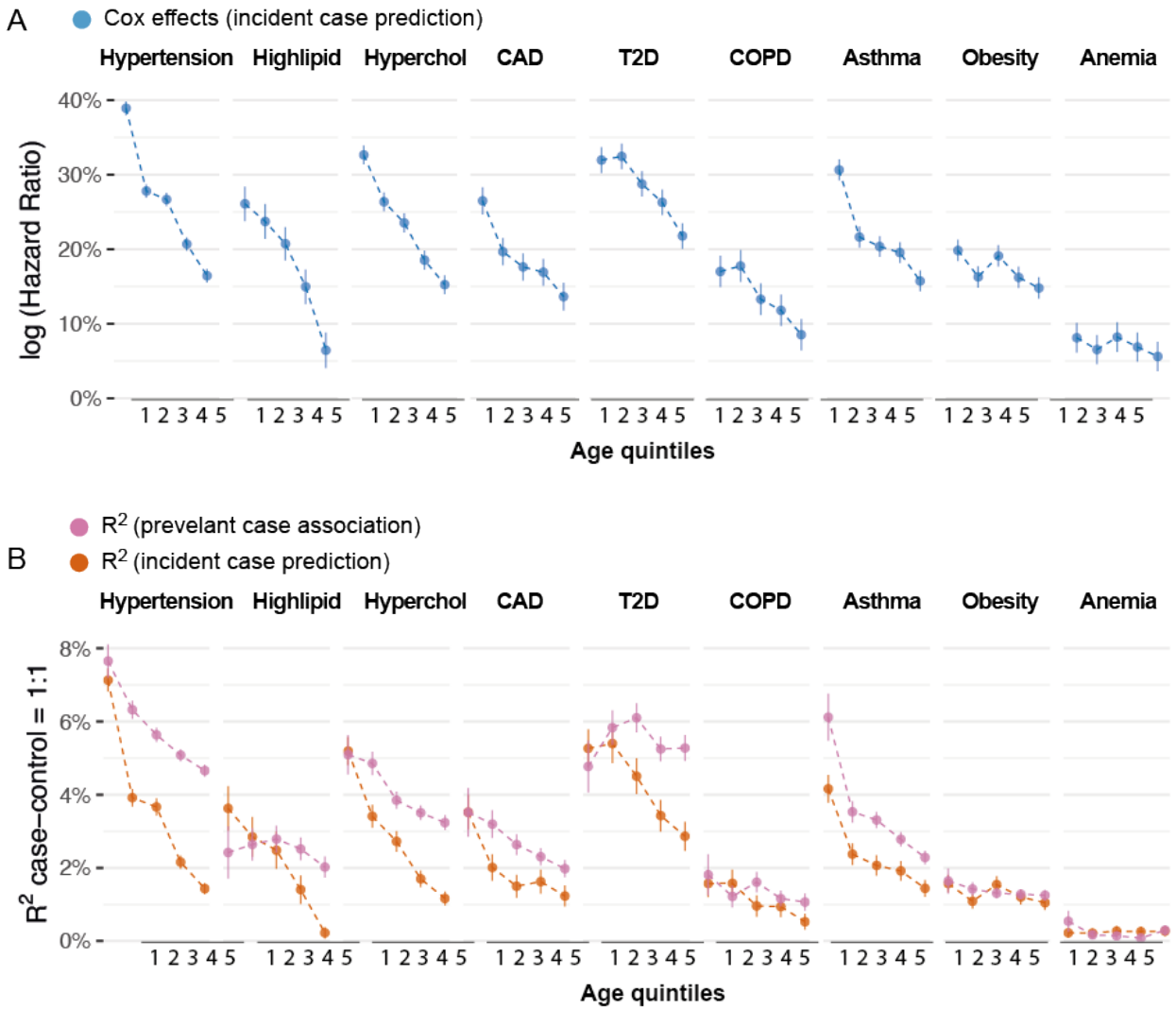

Figure 5: Age-dependent incident case prediction accuracy in 9 diseases. (A) Cox log hazard ratio of PRS on 9 diseases across 5 age quintiles. Each age bin has the same number of cases and 1:1 case-control ratio. Bars show standard error. (B) Age-dependent incident case prediction compared to prevalent case association accuracy in 9 diseases. Numerical results are provided in **Supplementary Table 13-14**.

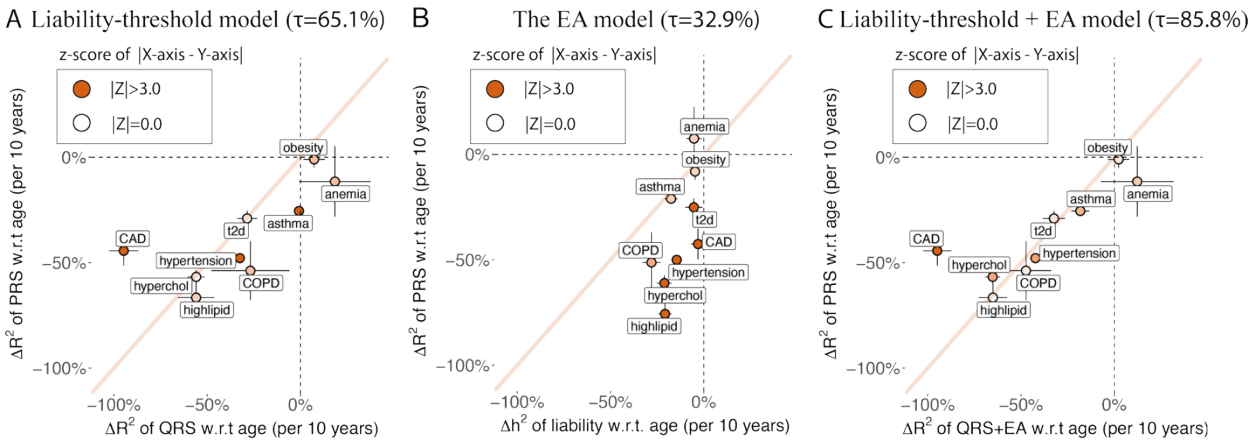

Figure 6: Liability-threshold model and the EA model explain age-dependent PRS prediction accuracy. (A) 10-year change in QRS prediction R^2 under the liability-threshold model versus 10-year change in PRS prediction R^2 for 9 disease traits. (B) 10-year heritability change in estimated disease liability versus 10-year change in PRS prediction R^2 for corresponding disease traits. (C) 10-year change in QRS prediction R^2 under the liability-threshold+EA model versus 10-year change in PRS prediction R^2 for 9 disease traits. Diagonal line has slope equals to 1. Bars show the se and color shows the z-score of difference in X and Y values of each dot. τ is the proportion of observed decrease in PRS accuracy explained by each model (**Methods**). Numerical results are provided in **Supplementary Table 15-17**. We note that no estimates are significantly outside the plausible range and that allowing estimates outside of the plausible range is necessary to ensure unbiasedness of estimates.

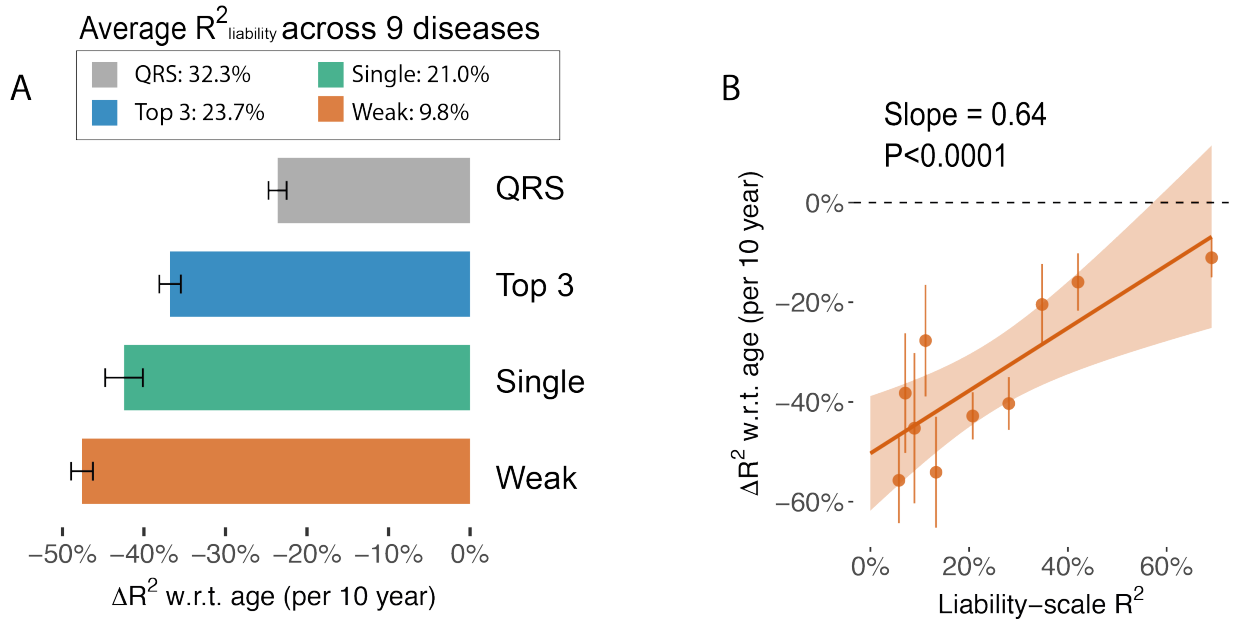

Figure 7. Risk models with higher liability-scale R^2 are less attenuated when predicting late-onset diseases. (A) Age-dependent prediction accuracy of predictors averaged across 9 diseases. X-axis shows the per-10-year change of prediction R^2 computed in 1-1 case control matching groups. QRS: predicted liability using 36 quantitative traits. Top 3: linear predictors use the top three quantitative traits that have the highest correlation with the diseases. Single (Strong): using a single quantitative trait to predict incident diseases, averaged across the top three traits as in the "Top 3" group; Single (Weak): the average between 4th and 5th predictor of each disease. (B) Scatter plot comparing the liability-scale R^2 (without age stratification) with the change of R^2 w.r.t. age across predictor-disease pairs. Predictor-disease pairs are grouped into 10 deciles based on liability-scale R^2 for visualization. The red line shows a regression line with confidence interval. Numerical results are provided in **Supplementary Table 18-19**.

852
853
854 **References:**

855 1. Simino, J. *et al.* Gene-age interactions in blood pressure regulation: a large-scale
856 investigation with the CHARGE, Global BPgen, and ICBP Consortia. *Am. J. Hum. Genet.*
857 **95**, 24–38 (2014).
858 2. Robinson, M. R. *et al.* Genotype-covariate interaction effects and the heritability of adult
859 body mass index. *Nat. Genet.* **49**, 1174–1181 (2017).
860 3. Winkler, T. W. *et al.* Genetic-by-age interaction analyses on complex traits in UK Biobank
861 and their potential to identify effects on longitudinal trait change. *Genome Biol.* **25**, 300
862 (2024).
863 4. Miao, J. *et al.* PIGEON: a statistical framework for estimating gene-environment interaction
864 for polygenic traits. *Nat. Hum. Behav.* 1–15 (2025).
865 5. Zhu, C. *et al.* Amplification is the primary mode of gene-by-sex interaction in complex
866 human traits. *Cell Genomics* **3**, (2023).
867 6. Jiang, X., Holmes, C. & McVean, G. The impact of age on genetic risk for common
868 diseases. *PLoS Genet.* **17**, e1009723 (2021).
869 7. Sakaue, S. *et al.* Trans-biobank analysis with 676,000 individuals elucidates the association
870 of polygenic risk scores of complex traits with human lifespan. *Nat. Med.* **26**, 542–548
871 (2020).
872 8. Jukarainen, S. *et al.* Genetic risk factors have a substantial impact on healthy life years. *Nat.*
873 *Med.* **28**, 1893–1901 (2022).
874 9. Dahl, A. *et al.* A Robust Method Uncovers Significant Context-Specific Heritability in
875 Diverse Complex Traits. *Am. J. Hum. Genet.* **106**, 71–91 (2020).

876 10. Pazokitoroudi, A. *et al.* A scalable and robust variance components method reveals insights
877 into the architecture of gene-environment interactions underlying complex traits. *Am. J.*
878 *Hum. Genet.* **111**, 1462–1480 (2024).
879 11. Thompson, D. J. *et al.* A systematic evaluation of the performance and properties of the UK
880 Biobank Polygenic Risk Score (PRS) Release. *PLoS One* **19**, e0307270 (2024).
881 12. Argentieri, M. A. *et al.* Integrating the environmental and genetic architectures of aging and
882 mortality. *Nat. Med.* **31**, 1016–1025 (2025).
883 13. Durvasula, A. & Price, A. L. Distinct explanations underlie gene-environment interactions
884 in the UK Biobank. *Am. J. Hum. Genet.* **112**, 644–658 (2025).
885 14. Zaitlen, N. *et al.* Informed conditioning on clinical covariates increases power in case-
886 control association studies. *PLoS Genet.* **8**, e1003032 (2012).
887 15. Pedersen, E. M. *et al.* Accounting for age of onset and family history improves power in
888 genome-wide association studies. *Am. J. Hum. Genet.* **109**, 417–432 (2022).
889 16. Aschard, H., Zaitlen, N., Lindström, S. & Kraft, P. Variation in predictive ability of
890 common genetic variants by established strata: the example of breast cancer and age.
891 *Epidemiology* **26**, 51–58 (2015).
892 17. Loh, P.-R. *et al.* Efficient Bayesian mixed-model analysis increases association power in
893 large cohorts. *Nat. Genet.* **47**, 284–290 (2015).
894 18. Weissbrod, O. *et al.* Leveraging fine-mapping and multipopulation training data to improve
895 cross-population polygenic risk scores. *Nat. Genet.* **54**, 450–458 (2022).
896 19. Fry, A. *et al.* Comparison of sociodemographic and health-related characteristics of UK
897 Biobank participants with those of the general population. *Am. J. Epidemiol.* **186**, 1026–
898 1034 (2017).

899 20. Tibshirani, R. Regression shrinkage and selection via the lasso. *Journal of the royal*
900 *statistical society series b-methodological* **58**, 267–288 (1996).
901 21. Udler, M. S. *et al.* Type 2 diabetes genetic loci informed by multi-trait associations point to
902 disease mechanisms and subtypes: A soft clustering analysis. *PLoS Med.* **15**, e1002654
903 (2018).
904 22. Jiang, X. *et al.* Age-dependent topic modeling of comorbidities in UK Biobank identifies
905 disease subtypes with differential genetic risk. *Nat. Genet.* **55**, 1854–1865 (2023).
906 23. Suzuki, K. *et al.* Genetic drivers of heterogeneity in type 2 diabetes pathophysiology.
907 *Nature* 1–11 (2024).
908 24. Celentano, D. D., Szklo, M. & Farag, Y. *Gordis Epidemiology*. (Elsevier - Health Sciences
909 Division, Philadelphia, PA, 2024).
910 25. Khera, A. V. *et al.* Genome-wide polygenic scores for common diseases identify individuals
911 with risk equivalent to monogenic mutations. *Nat. Genet.* **50**, 1219–1224 (2018).
912 26. Ge, T., Chen, C.-Y., Ni, Y., Feng, Y.-C. A. & Smoller, J. W. Polygenic prediction via
913 Bayesian regression and continuous shrinkage priors. *Nat. Commun.* **10**, 1776 (2019).
914 27. Privé, F., Arbel, J. & Vilhjálmsson, B. J. LDpred2: better, faster, stronger. *Bioinformatics*
915 **36**, 5424–5431 (2021).
916 28. Zheng, Z. *et al.* Leveraging functional genomic annotations and genome coverage to
917 improve polygenic prediction of complex traits within and between ancestries. *Nat. Genet.*
918 **56**, 767–777 (2024).
919 29. SCORE2 working group and ESC Cardiovascular risk collaboration. SCORE2 risk
920 prediction algorithms: new models to estimate 10-year risk of cardiovascular disease in
921 Europe. *Eur. Heart J.* **42**, 2439–2454 (2021).

922 30. Patel, A. P. *et al.* A multi-ancestry polygenic risk score improves risk prediction for
923 coronary artery disease. *Nat. Med.* **29**, 1793–1803 (2023).
924 31. Lee, S. H., Goddard, M. E., Wray, N. R. & Visscher, P. M. A better coefficient of
925 determination for genetic profile analysis. *Genet. Epidemiol.* **36**, 214–224 (2012).
926 32. Chatterjee, N., Shi, J. & García-Closas, M. Developing and evaluating polygenic risk
927 prediction models for stratified disease prevention. *Nat. Rev. Genet.* **17**, 392–406 (2016).
928 33. Torkamani, A., Wineinger, N. E. & Topol, E. J. The personal and clinical utility of
929 polygenic risk scores. *Nat. Rev. Genet.* **19**, 581–590 (2018).
930 34. Kullo, I. J. *et al.* Polygenic scores in biomedical research. *Nat. Rev. Genet.* **23**, 524–532
931 (2022).
932 35. Kullo, I. J. Promoting equity in polygenic risk assessment through global collaboration. *Nat.*
933 *Genet.* **56**, 1780–1787 (2024).
934 36. Genomic data in the All of Us Research Program. *Nature* 1–7 (2024).
935 37. Dempster, E. R. & Lerner, I. M. Heritability of threshold characters. *Genetics* **35**, 212–236
936 (1950).
937 38. Wray, N. R. & Goddard, M. E. Multi-locus models of genetic risk of disease. *Genome Med.*
938 **2**, 10 (2010).
939 39. Lee, S. H., Wray, N. R., Goddard, M. E. & Visscher, P. M. Estimating missing heritability
940 for disease from genome-wide association studies. *Am. J. Hum. Genet.* **88**, 294–305 (2011).
941 40. Witte, J. S., Visscher, P. M. & Wray, N. R. The contribution of genetic variants to disease
942 depends on the ruler. *Nat. Rev. Genet.* **15**, 765–776 (2014).

943 41. Hujoel, M. L. A., Gazal, S., Loh, P.-R., Patterson, N. & Price, A. L. Liability threshold
944 modeling of case-control status and family history of disease increases association power.
945 *Nat. Genet.* **52**, 541–547 (2020).
946 42. Hujoel, M. L. A., Loh, P.-R., Neale, B. M. & Price, A. L. Incorporating family history of
947 disease improves polygenic risk scores in diverse populations. *Cell Genom.* **2**, 100152
948 (2022).
949 43. Pedersen, E. M. *et al.* ADuLT: An efficient and robust time-to-event GWAS. *Nat. Commun.*
950 **14**, 5553 (2023).
951 44. Wu, P. *et al.* Mapping ICD-10 and ICD-10-CM Codes to Phecodes: Workflow
952 Development and Initial Evaluation. *JMIR Med Inform* **7**, e14325 (2019).
953 45. Kofink, D. *et al.* Statin Effects on Metabolic Profiles: Data From the PREVEND IT
954 (Prevention of Renal and Vascular End-stage Disease Intervention Trial). *Circ. Cardiovasc.*
955 *Genet.* **10**, (2017).
956 46. Wu, J. *et al.* A summary of the effects of antihypertensive medications on measured blood
957 pressure. *Am. J. Hypertens.* **18**, 935–942 (2005).
958 47. Esposito, K., Chiodini, P., Bellastella, G., Maiorino, M. I. & Giugliano, D. Proportion of
959 patients at HbA1c target <7% with eight classes of antidiabetic drugs in type 2 diabetes:
960 systematic review of 218 randomized controlled trials with 78 945 patients. *Diabetes Obes.*
961 *Metab.* **14**, 228–233 (2012).
962 48. Bulik-Sullivan, B. K. *et al.* LD Score regression distinguishes confounding from
963 polygenicity in genome-wide association studies. *Nat. Genet.* **47**, 291–295 (2015).
964 49. Friedman, J., Hastie, T. & Tibshirani, R. Regularization paths for generalized linear models
965 via coordinate descent. *J. Stat. Softw.* **33**, 1–22 (2010).

50. Tay, J. K., Narasimhan, B. & Hastie, T. Elastic net regularization paths for all generalized linear models. *J. Stat. Softw.* **106**, 1–31 (2023).